Renewable Energy 203 (2023) 382–393

Contents lists available at ScienceDirect

Renewable Energy

journal homepage: www.elsevier.com/locate/renene

Liquefaction, cracking and hydrogenation of microalgae biomass resources to CO_2 negative advanced biofuels: Mechanisms, reaction microkinetics and modelling

Dana Marinič [a,b], Miha Grilc [a], Brigita Hočevar [a], Florian Delrue [c], Blaž Likozar [a,b,*]

[a] Department of Catalysis and Chemical Reaction Engineering, National Institute of Chemistry, Hajdrihova 19, 1000, Ljubljana, Slovenia
[b] Faculty of Chemistry and Chemical Engineering, University of Maribor, Smetanova ulica 17, 2000, Maribor, Slovenia
[c] MicroAlgae Processes Platform, CEA, CEA Tech Région Sud - Provence-Alpes Côte d'Azur, F-13108, Saint Paul lez Durance, France

ARTICLE INFO

Keywords:
Microalgae
Biofuel
Liquefaction
Hydrodeoxygenation
One-pot reaction

ABSTRACT

Deoxygenation of triglycerides is one of the crucial pathways for the production of oxygen-free hydrocarbons and biofuels that are fully compatible with conventional internal combustion engines. The one-step liquefaction and hydrotreatment of *Chlorella sorokiniana* microalgae was investigated in a three-phase slurry reactor. The production of diesel-like hydrocarbons was successfully accomplished over sulfide form of $NiMo/Al_2O_3$ catalyst under hydrogen atmosphere. The present work contains a comprehensive investigation of the temperature and hydrogen pressure influence on the final product composition. The highest yield of C18 and C16 (26.1% and 10.7%, respectively) was reached by increasing the reaction temperature to 350 °C and hydrogen pressure to 50 bar, while at milder conditions (200 °C and 20 bar) the products appeared only in trace concentrations. In order to obtain an accurate kinetic model, reaction mechanism was first needed to be determined based on experimentally obtained products and intermediates. A simplified reaction pathway contains liquefaction, hydrogenolysis, hydrodeoxygenation, decarboxylation and decarbonylation. The model comprises mass transfer phenomena involved in the liquefaction process, the mass transfer of hydrogen from gas to liquid phase, adsorption, desorption and surface reaction kinetics. The lowest rate constant was calculated for the microalgae conversion to triglycerides ($k_0 = 1.93 \times 10^{-6}$ min^{-1}), indicating slow liquefaction.

1. Introduction

Environmental problems along with the rapid growth of energy demand, violent fluctuation of fuel price and limited fossil fuel reserves have led to the growing interest in renewable fuels. Expensive raw materials, which are responsible for 70–95% [1] of the total biodiesel cost, are one of the main reasons for the higher price compared to petroleum fuels and hence limited commercial use [2]. To minimize the human impact on the environment and nature, it is vital to further explore possible new natural and underutilized resources, while also to developing and improving the bio-fossil production technology.

Microalgal biomass was recognized as a prosperous feedstock for biofuel production. Due to its high biomass productivity, photosynthetic efficiency and high growth rate [3], it is deemed as a potential third generation biodiesel source. Moreover, microalgae have high accumulation capacity of lipids and fatty acids [4], which are the main energy source for biofuels. Food-based biofuels have raised a lot of concerns due to the moral issues. On the other hand, microalgae can grow on waste, marine water or wastewater, they do not require arable land, hence, do not compete with the food industry [5]. Lower greenhouse gases generation and consequently low carbon footprint of algae based biofuels [5] additionally boost academic and industry interest in this example of a circular economy. The advantage of having high tolerance to CO_2, makes microalgae a promising organism for CO_2 mitigation. 1.83 kg of CO_2, one of the most significant greenhouse gases, can be captured per 1 kg of cultivated microalgae. The biofuel produced from microalgae is considered carbon neutral, as the CO_2 produced from the biomass combustion can be further used as a fuel for the organism's metabolic activities in the cultivation process [6].

The technology of algal biofuel production has been developed greatly after 2010 [7], but still needs further elaboration and improvement in production, conversion and processing field [8]. Large-scale

* Corresponding author.Department of Catalysis and Chemical Reaction Engineering, National Institute of Chemistry, Hajdrihova 19, 1000, Ljubljana, Slovenia.
E-mail address: blaz.likozar@ki.si (B. Likozar).

https://doi.org/10.1016/j.renene.2022.12.055
Received 27 June 2022; Received in revised form 19 October 2022; Accepted 14 December 2022
Available online 16 December 2022

microalgae production is yet unfeasible due to its pricey cultivation and harvesting steps and high production cost. In addition, the bio-crude quality is unsatisfactory and the continuous operation is highly recommended to be elaborated on [9–11].

A typical pathway to converting microalgae biomass into biofuel involves a two-step process. Solid biomass is firstly processed into bio-crude and subsequently upgraded by catalytic hydrotreatment. The three main approaches used for the biocrude production are the lipid extraction and further transesterification, pyrolysis and the hydrothermal liquefaction (HTL) [8]. The first process is the most studied [9] and currently the most common [12] algae biofuel production pathway. However, the process is not economically profitable with poor lipid extraction selectivity [10]. The latter stands out due to its practicality because of the algal high water content [8]. In comparison to HTL, which can convert biomass with high moisture content (above 50% mass fraction) [9], pyrolysis can decompose only dry organic feedstock [4]. Further studies revealed that HTL has lower carbon footprint, a better energy return on investment and higher economic potential in comparison to the two previously mentioned methods [13]. Direct use of bio-crude is not fully compatible with conventional diesel engines due to its high oxygen content [14]. Oxygen rich biofuels have low heating value, high viscosity at room temperature [15] and poorer flow property [8]. Its high content leads to corrosion, incomplete burning [10] and thermal instability [15], hence the further hydrotreatment is necessary.

Oxygen is selectively removed from fatty acids (FA), fatty acid methyl esters (FAME) and other oxygen containing compounds typically in a form of water via direct hydrodeoxygenation (HDO), CO via decarbonylation (DCN) or CO_2 via decarboxylation (DCX) [16]. The first potential pathway yield hydrocarbons with the same number of carbon atoms as the corresponding FA bound in the original triglycerides (TG), whilst the latter two yield C_{n-1} hydrocarbons [17,18].

Extensive efforts have been made in the past to investigate the HDO reaction pathway for FAs (stearic [1,19], palmitic [20], lauric acid), FAME [1,21] and unnatural TG [1,12,17,21]. Literature studies [17,22] report that the HDO of TG starts with hydrogenation of unsaturated FA units. Further hydrogenolysis results in three FAs and a propene moiety as a side product. The following hydrogenation reduce carboxyl group in FA to aldehyde group, which is rapidly reduced to alcohol and further to aliphatic hydrocarbon. Other possible reactions involved in the catalytical hydrotreatment are isomerization, cyclization, cracking and aromatization.

Several (micro)kinetic models for intermediates have already been developed. Arora et *al.* [19] developed a kinetic model for HDO of stearic acid, while Yenumala et *al.* [17] and Hachemi and Murzin [21] studied the HDO kinetics of FAME and TG. Agarwal et al. [23] developed a molecular-level kinetic model for hydroprocessing of TG, which consisted of 8–22 carbon fatty acids. The final network contained 476 species and 1709 reactions.

However, studies on the microalgae conversion to n-paraffins remains elusive. To fill this gap, we developed the first kinetic model based on the reaction mechanisms proposed from the experimental results that considers one-pot microalgae biomass liquefaction, DCN, DCX and HDO. Microalgae, with the total lipid content 28.5 ± 0.4%, were transformed into a mixture of diesel-like hydrocarbons over commercial bifunctional NiMo/γ-Al_2O_3 catalyst. Relevant kinetic parameters obtained by the regression analysis allowed the prediction of the optimal process conditions for yielding n-paraffins and can be used for process optimization.

Moreover, additional treatment leads to the time, energy and cost prohibitive processes. Reduction of the cost of algae-based biofuels is necessary to reach its relative competitiveness with fossil fuels. In pursuance of sustainable future, the main goal of this study was the one-pot algae conversion into biofuel by simultaneous liquefaction and catalytic hydrotreatment, which eliminates the extra steps required for catalytic upgrading. The influence of several parameters, like the temperature, pressure, reaction time and catalyst form on the product composition was established.

2. Material and methods

2.1. Catalyst preparation and characterization

A commercially available bifunctional NiMo/γ-Al_2O_3 was used for hydrodeoxygenation. The catalyst was received in oxide form and was sulfided prior to use by the dimethyl disulfide (DMDS) sulfiding agent. The sulphided form of the catalyst was chosen for experimental work as it was showed to be by far most suitable, due to its high activity in comparison with the oxidized and reduced form, investigated in our previous work [24], regarding hydrodeoxygenation and hydrocracking of lignocellulosic biomass. Moreover, this form is known to be frequently used in petro-industry [24].

The catalyst was first dried in a N_2-purged (200 mL min^{-1}) furnace at 200 °C for 2 h. The reactor was filled with 15 g of dried catalyst, 20 mL of n-hexane (≥99%, Sigma–Aldrich) and 3 g of DMDS (≥99%, Sigma–Aldrich) sulfiding agent. The reactor was sealed and purged with nitrogen (5.0, Messer) three times and pressurized to 2.5 MPa of H_2 (5.0, Messer). The reaction mixture was heated-up to 350 °C at the heating rate of 5 °C min^{-1} by an electric jacket heater. After keeping the reaction content at the desired temperature for 90 min, the reactor was cooled-down, depressurized and flushed with nitrogen overnight (200 L min^{-1}). The catalyst was sulfided in pelletized form and grinded and sieved to fractions of 40–100 μm prior the reactions. Oxidized and reduced catalyst form were also studied in this research paper. The catalyst reduction was performed in a H_2-purged (200 mL min^{-1}) reduction oven at 400 °C for 3 h.

The catalyst characterization was thoroughly discussed in our previous works [25,26]. The concentration of the active sites after the sulfidation was determined to be 0.33 μmol m^{-2} (by consecutive H_2-TPR, O_2-TPO and H_2-TPR experiments), the surface area was 170 m^2 g^{-1} (by the Braunauer–Emmett–Teller method (BET) using ASAP 2020 instrument for N_2-physisorption), pore volume 0.471 cm^3 g^{-1} and pore size 8.9 nm. The structural characterization of fresh catalyst was determined by different characterization methods (SEM, EDX and XRD) in our previous papers [24,27]. The same methods were used for the characterization of the spent catalyst. The transmission electron microscope (TEM) Jeol JEM 2100 operated at 200 kV was used to observe the fresh and used catalyst, deposited on a copper-grid-supported lacy carbon foil. The chemical composition was analysed using a Jeol JED 2300 EDXS system. To explore the acidic properties of sulfided NiMo catalyst, the temperature programmed desorption of ammonia (NH_3-TPD) was employed using the Micrometrics AutoChem II Chemisorption Analyser (Micrometrics, Norcross, GA, USA). The catalysts were pretreated in an Ar atmosphere at 350 °C for 2 h. The materials were treated with 10% NH_3 in He (5.0, Messer) for 1 h and purged with pure He for another hour. Ammonia temperature programmed reaction was carried out up to 600 °C in pure He.

2.2. Biomass characterization

Microalgae cultivation, harvesting and lipid extraction was done by CEA, DSUD, Cadarache, France. The microalgae species used in this study was *Chlorella sorokiniana* NIES 2173. The most relevant characteristics are presented in Table 1. Qualitative and quantitative FAME (fatty acids methyl esters) profile is shown in Table 2. The FAME are labeled as ''Cx:y'', where x indicates the number of carbon atoms and y the number of double bonds. Microalgae were stored at 5 °C before use.

2.3. Catalytic hydrotreatment

The catalytic hydrotreatment of *Chlorella sorokiniana* was performed in a 300 mL cylindrical stainless-steel slurry reactor (Parker Autoclave Engineers) equipped with a Rushton turbine impeller. The reactor was filled with 120 mL of reaction mixture that contained 5 wt% of algae, the rest being dodecane (≥99%, TCI). The solvent had also a cooling

Table 1
Properties of biomass feedstock.

Characteristic	%
Dry-weight content	39
Total lipid content[a]	28.5 ± 0.4
Total carbohydrate content[b]	40.1 ± 3.6
Nitrogen content[c]	4.08
Protein content[d]	20.6

[a] Determined by an adapted Folch method [31].
[b] Determined by Dubois method [32].
[c] Determined using a FLASH 2000 (ThermoFisher Scientific, USA) CHNOS analyzer.
[d] Calculated based on the N-to-protein conversion factor of 5.04 [33].

function, since the hydrotreatment is exothermal. Commercially available NiMo/γ-Al_2O_3 catalyst in reduced, oxidized and sulfide form was used in this study. The catalyst mass was set to 25 wt% with regard to the initial mass of microalgae. The system was sealed and purged twice with nitrogen (5.0, Messer) to ensure inert gaseous headspace. The initial H_2 (5.0, Messer) pressure was adjusted to 20, 30 or 50 bar. The reaction mixture was heated-up by increasing the temperature from room temperature to the desired reaction temperature with a heating ramp of 5 °C min^{-1} (see Table 3). Experiments were carried out in batch regime with agitation speed of 1000 min^{-1}. The reaction conditions were held constant for 4 h. After the rapid cool down, the decompressed gas phase from the reactor was analysed by micro-GC (Agilent 490 Micro GC, TCD detectors equipped with PoraPLOT U and CP-COx columns). Before opening, the reactor was purged with nitrogen. The catalyst and the residue were separated from the reaction mixture by filtration. The solid samples collected from the filtration were washed three times with dodecane and once with n-hexane (≥99%, Merck), then dried in the oven overnight at 100 °C. The solid residue was washed with ethanol and dried before being further characterized by Fourier Transform Infrared Spectroscopy (FTIR, Spectrum Two FT-IR spectrometer, PerkinElmer, Waltham, USA), SEM, EDX, TEM and XRD. The liquid samples collected from the filtration were analysed undiluted by Gas Chromatography – Mass spectroscopy (GC-MS, Shimadzu Ultra 2010) and by FTIR.

2.4. Analysis of the liquid phase

Liquid samples were collected through the sampling line 30 min after reaching the reaction temperature and in 30- or 60-min intervals onward. Sampling prior to 30 min after reaching the reaction temperature was not possible due to the possibility of clogging the sampling line with the unliquefied microalgae, especially at lower temperatures. The unknown components were identified using GC-MS (Ultra 2010, Shimadzu, Kyoto, Japan) according to the mass spectrum and the retention index matching with the standards form NIST 14 and FFNSC 2 libraries. For the quantification, the flame ionization detector GC–FID (Focus GC, Thermo Scientific, MA, USA) was used. The products (injection volume 1 μL, injector temperature 300 °C, split ratio 50) were separated on capillary column ZB-5MS (60 m × 0.25 mm × 0.25 μm, Phenomenex, Torrance, CA, USA) while subjected to the set temperature program (5.5 min at 60 °C, 60 °C–320 °C at 20 °C min^{-1}, 21.5 min at 320 °C). In order to calculate the concentrations, a five-point calibration curve was done with high purity external standards for all quantified components. All standards were purchased from Sigma–Aldrich.

Table 2
Fatty Acid Methyl Esters profile of Chlorella sorokiniana determined by an adapted Folch method.

FAME	C14:0	C16:0	C16:1	C17:0	C17:1	C18:0	C18:1	C18:2	C18:3	Others
Total lipids (%)	1.31	10.44	2.02	1.57	0.89	7.77	11.04	32.18	10.64	22.15

Table 3
Reaction conditions for each run.

Run	Catalyst form	T[a] (°C)	P[b] (bar)	W_{cat} (wt%)	Reaction time (h)[g]
1	Sulfided NiMo/γ-Al_2O_3	200	50[c]	25	4
2	Sulfided NiMo/γ-Al_2O_3	300	50[c]	25	4
3	Sulfided NiMo/γ-Al_2O_3	312	50[c]	25	4
4	Sulfided NiMo/γ-Al_2O_3	325	50[c]	25	4
5	Sulfided NiMo/γ-Al_2O_3	350	50[c]	25	4
6	Sulfided NiMo/γ-Al_2O_3	325	20[c]	25	4
7	Sulfided NiMo/γ-Al_2O_3	325	30[c]	25	4
8	Sulfided NiMo/γ-Al_2O_3	350	20[c]	25	4
9	Sulfided NiMo/γ-Al_2O_3	350	30[c]	25	4
10	Sulfided NiMo/γ-Al_2O_3	325	50[d]	25	4
11	Sulfided NiMo/γ-Al_2O_3	350	50[d]	25	4
12	oxided NiMo/γ-Al_2O_3	325	50[c]	25	4
13	reduced NiMo/γ-Al_2O_3	325	50[c]	25	4
14	/	325	50[c]	0[e]	4
15	Sulfided NiMo/γ-Al_2O_3	325	50[c]	25[f]	4
16	Sulfided NiMo/γ-Al_2O_3	350	50[c]	25	0[h]
17	Sulfided NiMo/γ-Al_2O_3	350	50[c]	25	1
18	Sulfided NiMo/γ-Al_2O_3	350	50[c]	25	2
19	Sulfided NiMo/γ-Al_2O_3	350	50[c]	25	3
20	Sulfided NiMo/γ-Al_2O_3	350	50[c]	25	5

[a] Set temperature at the plateau.
[b] Initial pressure in reactor.
[c] Hydrogen atmosphere.
[d] Nitrogen atmosphere.
[e] Blank – no catalyst.
[f] Blank – no algae.
[g] At the plateau temperature.
[h] 20 min before reaching the final temperature.

2.5. Fourier-transform infrared spectroscopy analysis

The infrared spectrometry analysis was performed using Spectrum Two FT-IR spectrometer (PerkinElmer, Waltham, USA). The spectra were collected in the range 4000–400 cm^{-1} using a scan speed of 64 scans per second.

3. Results and discussion

3.1. Catalyst characterization

Although the same catalyst was already thoroughly characterized in our previous works [25–27], the quantification of acidic properties of sulfided NiMo catalyst was performed to estimate the active sites concentration. The total quantities of acid sites on the catalyst calculated from NH_3-TPD and integration of NH_3 desorption curve (Fig. S1) was 1.19 mmol g^{-1}.

X-ray diffraction (XRD) patterns of the fresh and used catalysts are presented in Fig. S2 and were used for structural characterization of the catalysts. From the diffraction profile of the fresh catalyst, only the peaks related to the Al_2O_3 support at the 2θ values of 36.6°, 46.0°, 59.1° and 66.6° can be perceived. The diffraction angles are referred to the diffraction of (3 1 1), (4 0 0), (5 1 1) and (4 4 0) Al_2O_3 planes, in the same order. Similar characteristics have also been reported by Liu et *al.* [28]. Spent catalysts exhibit lower crystallinity, indicated by an obvious decrease in the intensity of diffraction peaks characteristic for fresh catalyst. This can be explained by the presence of undiluted amorphous biomass in the sample. Several small peaks at diffraction angles in the range of 2θ = 10°–40° are seen and couldn't be identified due to the complex mixture of undiluted biomass.

SEM analysis was performed on the spent catalyst (Fig. 1b) in order to analyze the coke loading on the catalyst surface and possible remains of undiluted biomass in the sample. EDX mapping was also conducted in order to quantitatively analyze the coke distribution. As shown in Fig. S3, the surface of the used catalyst is covered with a layer of coke, which originates from the reaction components. The coverage of catalyst activity centers could lead to catalyst deactivation. The elemental analysis of solid residue showed, that although washed with polar and nonpolar solvents, it still comprises of undiluted biomass from microalgae with high carbon content (78.72%), whereas the carbon content on the spent catalyst was 13.3% (Table S1). Moreover, the average particle size after the reaction decreased, presumably because of its collision with the impeller and mechanical abrasion.

TEM analysis was performed for catalyst surface and structure analysis and was supplemented with EDXS analysis for chemical composition determination. Lower magnification image (Fig. 2a) shows fresh catalyst that consists of agglomerates of relatively small cubic alumina crystallites. At higher magnification (Fig. 2c) individual nanocrystallites of alumina can be perceived and are marked with red dashed line. Nanoparticles, approximately 1 nm in size, are uniformly

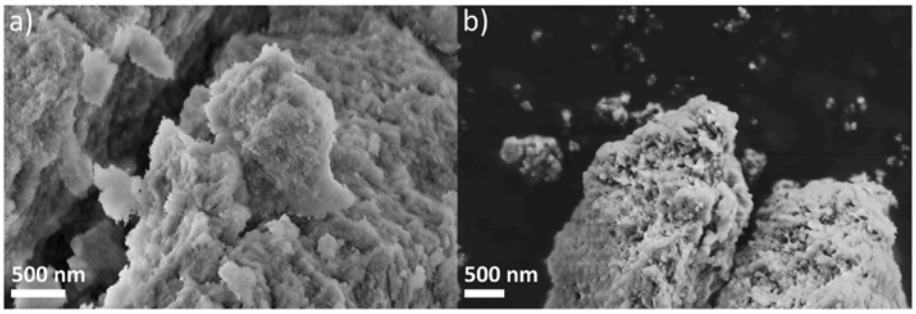

Fig. 1. SEM images of a) fresh catalyst and b) spent catalyst.

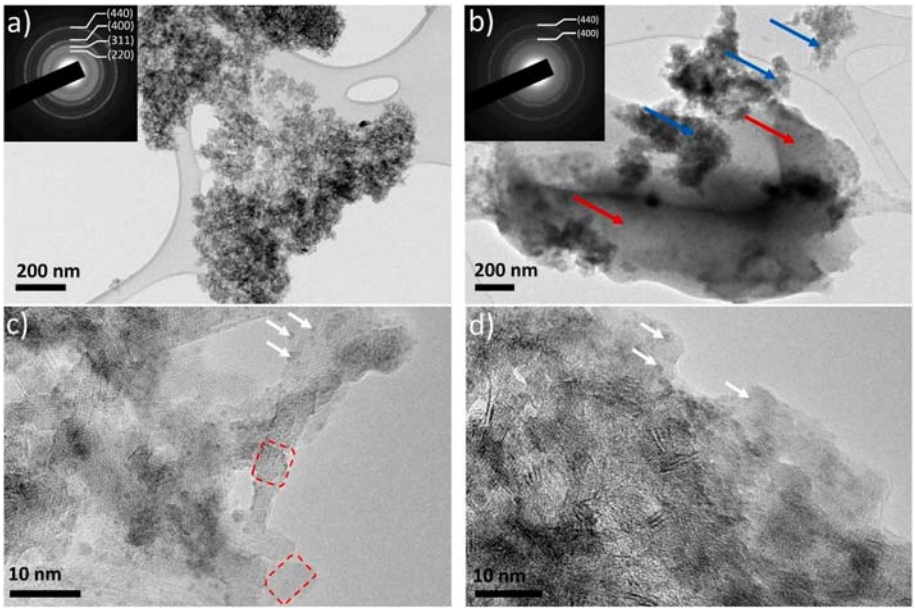

Fig. 2. TEM images of the fresh (a,c) and spent catalyst (b, d). Insets are Selected area electron diffraction patterns acquired from the catalyst's particles and indexed according to cubic Al_2O_3. Dashed red rectangular encircle alumina nanocrystals, white arrows show Ni/Mo nanoparticles, red arrows show undiluted biomass and blue arrows the catalyst.

decorating alumina crystallites. EDXS analysis on several parts, including areas where nanoparticles were clearly seen and are marked with white arrows, showed presence of Mo, Ni and S elements. Due to spatial resolution of EDXS analysis, which is larger than individual nanoparticle size, distinguishing Ni and Mo or NiMo alloyed particles is impossible. Thus, we can not clearly state whether the nanoparticle is Ni, Mo or NiMo. The Mo-L line and S–K line strongly overlap (peak separation less than resolution of spectrometer) which makes the distinguishing of these elements difficult. However, we confirmed the presence of Mo in the sample with Mo–K line which doesn't overlap with S.

The lower magnification image of solid residue after reaction (Fig. 2b) shows the presence of undiluted biomass (red arrow) and the catalyst (blue arrow), as already demonstrated by SEM analysis. TEM images and EDXS analysis identified homogenous dispersion of Ni and Mo nanoparticles across the support. No major alterations were observed in catalyst structure after the reaction. The Ni/Mo particle growth or agglomeration into larger particles was not perceived.

3.2. Algae characterization

The algal content greatly depends on several factors. It varies between the species, harvest and cultivation conditions [8]. Dry weight studies of *Chlorella sorokiniana* present typically a composition of 40% proteins, 30–38% carbohydrates and 18–22% lipids [29]. This research was performed using relatively low protein level strain (20.6%) of *Chlorella sorokiniana* NIES 2173 (Table 1). On the other hand, the relatively high lipid content of 28.5% gives elevated caloric value to the biomass. Yun et al. [30] determined the total lipid content for two *Sorokina* strains KNUA122 and KNUA114 to be up to 19.31% and 23.28%, respectively.

Fatty acids are responsible for 10–20% of the algae dry mass [30], and their abundance is of utmost importance for the efficient fuel production. While Yun et al. [30] showed the undistributed fatty acid composition, where only saturated and unsaturated C16 and C18 FA were determined, the microalgae in this study exhibited also a small proportion of C14 and C17 FA. They also confirmed the elevated saturation of FA at increased cultivation temperature. At 35 °C 40–50% of FA represented saturated FA, while in our case 73% of C14–C18 FA were composed of unsaturated FA.

3.3. Liquid phase analysis

The liquid samples collected during the reactions were identified by GC-MS and quantified by GC-FID. GC analysis gave insight into the oil composition which revealed, that the produced bio-oils are complex mixtures of partially or completely deoxygenated compounds.

Bio-oil composition highly depend on the biochemical composition of microalgae. Most microalgal triglycerides consist of three saturated, monounsaturated or polyunsaturated FA units (typically C14–C22) bonded to a propane moiety [12,15,34]. Most common polyunsaturated FAs are linoleic and linolenic acids [10]. Therefore, the product is a mixture of hydrocarbons and different intermediates, depending on the degree of deoxygenation and deoxygenation route [1,10].

Qualitative and quantitative Fatty Acid Methyl Esters profile (FAME) profile (Table 2) of *Chlorella sorokiniana* shows that it was mainly composed of C18 (7.77% C18:0, 11.04% C18:1, 32.18% C18:2, 10.64% C18:3) fatty acids. Heptadecane (C17) and octadecane (C18) were the two major products formed. It is known that green microalgae contain very little or no C17 FA [35]. High product yield of C17 can be therefore attributed to decarbonylation (DCN) of stearyl aldehyde and decarboxylation (DCX) of stearic acid, which yield hydrocarbons hydrocarbons with one carbon atom less than the reactant [17,18]. C18 is formed via hydrodeoxygenation (HDO) of stearic acid. The second most abundant FA bound in the original TG was palmitic acid (10.44% C16:0, 2.02% C16:1). Aliphatic hydrocarbons with 15 and 16 carbons were also present in the product mixture. C15–C18 n-paraffins are typical product mixtures produced from TG with heterogeneous catalytic hydrogenation [22].

Short chained hydrocarbons, such as alkanes ranging from C3 to C10, 2-methyl-butane, isobutane, 3-methyl-pentane, cyclization products such as cyclopentane, methyl-cyclopentane, 1-methyl-cyclopentene, cyclo-hexane, toluene, and oxygen compounds such as 2,5-dimethyl-furan and 2-methyl-furan were also identified in the samples. These compounds were present in extremely low or moderate concentrations relative to the product formation (maximum of 0.003 mol L^{-1} of n-hexane in the run 4) and are products of additional possible reactions involved in the catalytic hydrotreatment. Cracking, isomerization and cyclization are promoted by acidic sites on the catalyst support [18]. Cracking could also explain the decrease of the ratio of C16/C18 alkane chains from 1:5 to 1:2.3 in the initial feedstock and final product, respectively.

GC study of bio-oils produced at lower temperatures and lower hydrogen pressure reveals a great diversity in the product composition. Because of incomplete deoxygenation and hydrogenation, several intermediates are still present in the final product. These include stearyl alcohol, stearyl aldehyde, stearic acid, palmitic acid, hexadecanol, different isomers of pentadecane, hexadedcane, heptadecene and octadecene and several different undefined compounds. Despite the use of sulfided catalyst and microalgal sulfur content, no sulfur-containing compounds were detected. The reason probably lies in minor concentrations due to the presence of heteroatom removal catalyst [22]. Fig. 3 illustrates the GC-FID chromatogram of the most promising experiment at 350 °C and 50 bar of initial hydrogen pressure. It indicates almost complete deoxygenation, which results in more stable product.

The yields of produced oils are listed in Table 4 and were calculated according to Eq. (1). The effect of the process temperature, initial hydrogen pressure, catalyst form and processing time is notable and thoroughly discussed in Subsections 3.4, 3.5, 3.6 and 3.7.

$$\text{Yield\% of C15} - \text{C18} = \frac{\text{moles of product produced}}{\text{moles of corresponding FA in the feed}} \bullet 100 \qquad (1)$$

3.4. Effect of the process temperature

The influence of the process temperature on the liquefaction and hydrotreatment was investigated by conducting the experiments at 200, 300, 312, 325 and 350 °C under otherwise identical experimental conditions. The reactants' conversion rose exponentially (yield = $0.0007e^{0.0329\ T}$) with elevating temperature (Fig. 4) due to higher kinetic rates. These results are consistent with several different studies, which claimed the increased conversion of TG [14,36] and

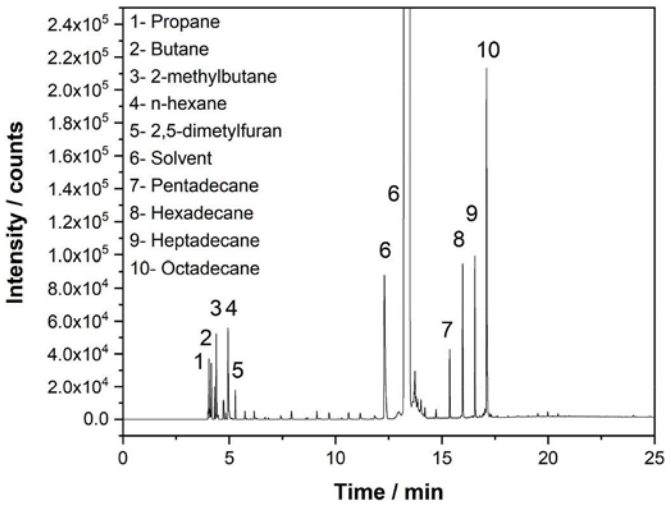

Fig. 3. GC-FID chromatogram of the product at reaction conditions of 350 °C and 50 bar of hydrogen pressure over sufided catalyst.

Table 4
Yields for C18–C15 alkanes and alkenes at different pressures and temperatures over sulfided catalyst.

Reaction conditions		Yield (%)			
T	*P*	C15	C16	C17	C18
200 °C	50 bar	0.02	0.11	0.10	0.24
300 °C	50 bar	1.35	1.48	2.73	4.70
312 °C	50 bar	4.75	4.90	9.69	11.17
325 °C	50 bar	4.64	6.13	9.61	14.94
350 °C	50 bar	5.12	10.65	10.36	26.08
325 °C	0 bar	0.31	0.11	0.32	0.23
325 °C	20 bar	4.64	4.34	9.30	10.14
325 °C	30 bar	5.87	6.46	12.28	14.48
350 °C	0 bar	0.38	0.16	0.32	0.30
350 °C	20 bar	4.02	4.14	7.44	9.35
350 °C	30 bar	4.83	6.65	9.02	14.91

hydrodeoxygenated product formation from model compounds when elevating the temperature and hydrogen pressure [19]. The solubility of hydrogen is determined by the temperature and pressure, therefore higher pressure and temperature increase the availability of gas in the reaction mixture [17]. A maximum yield of C18 with respect to the initial moles of FA in the feed was 26.08% and was obtained at the highest reaction temperature (350 °C) and hydrogen pressure (50 bar). The product formation at lower temperatures (200 °C) was neglectable. Nonetheless, the temperature rise accelerated cyclization, isomerization and hydrocracking reactions. Too high processing temperature could have led to overcracking [34], evidenced by elevated C3–C6 light hydrocarbon formation.

3.5. Effect of the processing hydrogen pressure

The reaction pressure variation between 20 and 50 bar influenced mostly the yield and product distribution. With an increase in hydrogen pressure from 30 to 50 bar at 350 °C, the yield of C15-18 alkanes increased from 21.0% to 52.5%, while the yield of alkenes decreased from 13.4% to 4.0% (Fig. 5). Hydrogen is essential for the conversion of microalgae, since it is needed for most of the reactions in the process. Furthermore Kim et al. [12] showed that increased unsaturation in triglycerides can increase the possibility of several side reactions and formation of heavy by-products, due to the catalyst deactivation. This results in lower yields of the aimed paraffins. They suggested

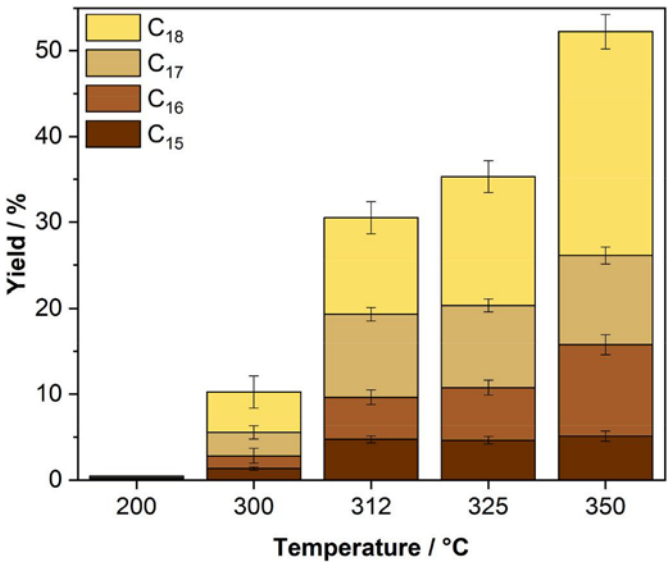

Fig. 4. The influence of the process temperature on the product yield at 50 bar of hydrogen pressure.

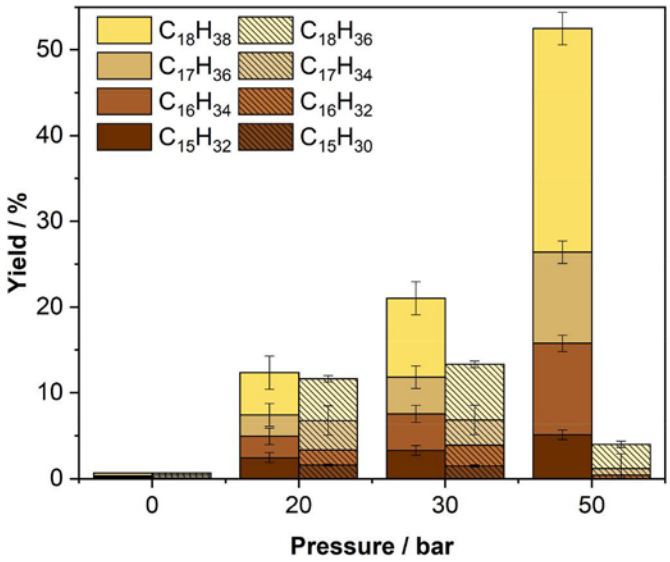

Fig. 5. The influence of the hydrogen pressure on the alkane and alkene distribution at 350 °C.

presaturation (pre-hydrogenation) of triglycerides at mild reaction temperatures. Due to the high proportion of unsaturated FAs present in the used microalgae, high hydrogen pressure for hydrogenation is necessary.

Even though saturation is usually a rapid process, analysis still revealed a significant amount of different isomers of alkenes in the product mixture produced at lower hydrogen pressures. Alkanes are potentially formed via dehydration of alcohol, as intermediates in the HDO process. At inferior presence of hydrogen pressure, the saturation of alkenes to alkanes cannot be fully reached. High unsaturation degree notably effects the oxidative stability of biodiesel, since the oxidation reactions start with the oxygen attack to the double carbon bonds. Very similar influence of the temperature has been reported by Arora et al. [19], however they found a weak dependence on pressure, which does not coincide with our results.

Furthermore, a parallel reaction with identical reaction conditions as the most promising experiment (run 5) but under inert (nitrogen) atmosphere was carried out in order to check the possibility of microalgae conversion to paraffins without hydrotreatment. The experiment revealed the importance of H_2 presence since it yielded no product formation.

Fig. 6 shows the concentration profile of the products as a function of reaction time at 350 °C and different H_2 pressures. At greater availability of hydrogen pressures the rate of formation of HDO product was faster than DCN and DCX product formation. The reason lies in the hydrogen needed for all of the intermediate reactions in the process.

3.6. Effect of the catalyst form

In the current study, the microalgae biomass was processed using NiMo/γ-Al_2O_3 catalyst. Hydroprocessing is generally and most commonly carried out over Al_2O_3 supported metal, while nickel and its modification with other metals, like Mo, exhibit high HDO activity and low cost [8]. However, Hachemi et *al.* [1] showed faster stearic acid conversion over H–Y zeolite supported Ni compared to alumina support. Sulfided form showed high activity during hydrotreatment, whereas oxidized and reduced form showed almost no activity. In the absence of catalyst, the conversion was found to be neglectable. Grilc et al. [24] reached a similar conclusion for the hydrodeoxygenation of liquefied lignocellulosic biomass. Nevertheless, many authors proved the high efficiency of nonsulfided catalyst for deoxygenation of fatty acids [19]. NiMo/γ-Al_2O_3 [37], carbon supported palladium catalyst [38], Ni

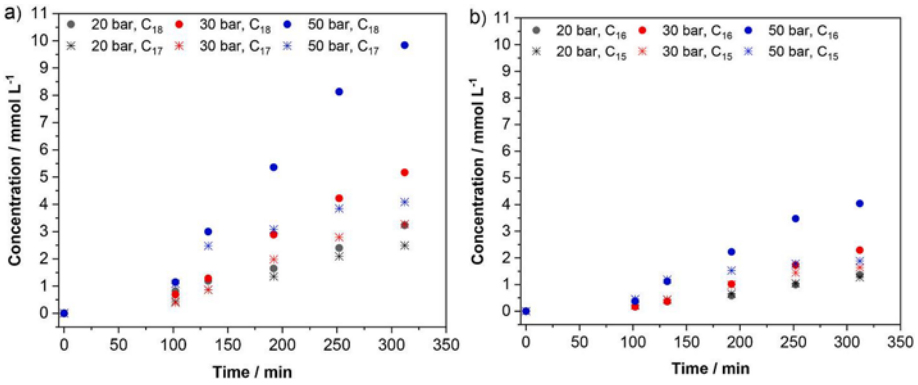

Fig. 6. The concentration profile of the products a) C18 and C17 and b) C16 and C15 as a function of reaction time at 350 °C and different H_2 pressures.

supported acidic zeolite (HZSM-5 and HBeta) [39], silica-supported Pd and PdAu [40] and palladium nanoparticles supported on a mesocellular silica support [41], exhibited high selectivity towards targeted n-paraffin, 80%, >98%, 84.6%, >93% and complete selectivity, respectively.

3.7. Effect of the processing time

The influence of the activity was investigated by conducting the experiments for 50 min (20 min before reaching the final temperature) and 1, 2, 3 and 5 h at the temperature of 350 °C and the hydrogen pressure of 50 bar. The algal biomass was, to a great extent, already liquefied within the first hour. After 3 h, the conversion (calculated from Eq. (3)) increased to 80% and the amount of insoluble residue (calculated from Eq. (2)) remained almost constant for the next 2 h, around 17 wt% (Fig. 7).

$$\text{Residue } (\%) = \frac{\text{weight of residue}}{\text{weight of algae}} \cdot 100 \tag{2}$$

$$\text{Conversion } (\%) = 100 - \text{residue} \tag{3}$$

3.8. Gas phase analysis

The gas products were mostly composed of H_2O, CO, CO_2 and light hydrocarbons such as CH_4, C_2H_6 and C_3H_8. The mmol of gas per gram of initial algae mass for run 5 was 0.54, 0.14, 0.18, 0.18, 0.11 and 0.05, respectively. From the gas product composition, we can again conclude

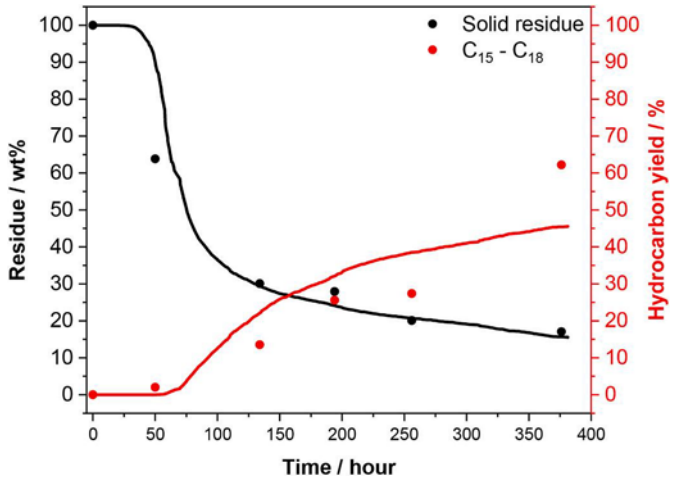

Fig. 7. Experimental data (●) and modeling results (lines) for the simultaneous liquefaction and hydrotreatment of microalgae biomass over the sulfide form of NiMo/γ-Al_2O_3 at 350 °C and 50 bar of hydrogen pressure.

that HDO (removal of O atoms as H_2O) is a more dominant deoxygenation pathway than DCN and DCX (removal of O atoms as CO and CO_2). HDO is preferable over DCN and DCX considering carbon economy and environment friendliness. The only side product is water, in place of indirect or direct culprits for global warming, CO and CO_2. Furthermore, it yields hydrocarbons with one more carbon number, which gives higher energy value [18].

The deoxygenation pathway is usually determined by the catalyst used [16]. Noble metal catalysts such as Pt and Pd favor DCN and DCX over HDO [12,15], while NiMo is being widely used in the petrochemical industry for HDO [24]. This can be explained by the catalyst's active sites. Decarbonylation proceeds on active metallic sites. Dehydration in HDO process occurs on the acidic sites of the catalyst and the following hydrogenation to alkanes on the metallic sites. Weak acidic NiMo/Al_2O_3 therefore prefers HDO over DCN and DCX [17].

Light hydrocarbons are products of hydrogenolysis of the glycerol moiety in the TG structure and hydrocracking [12,19]. Methane is additionally generated by methanation reaction of CO (Eq. (4)) and CO_2 (Eq. (5)). CO_2 is also produced due to the water gas shift reaction (Eq. (6)) [12,19]. Furthermore, sulfided catalyst usually produce more CO_2 than CO [15].

$$CO + 3H_2 \rightarrow CH_4 + H_2O \tag{4}$$

$$CO_2 + 4H_2 \rightarrow CH_4 + 2H_2O \tag{5}$$

$$CO + H_2O \leftrightarrow CO_2 + H_2 \tag{6}$$

3.9. FTIR analysis

The FTIR spectra of produced oils and solid residue are shown in Fig. 8a and b. Peaks seen on the spectra of bio-oils (Fig. 8a) correspond quite well with the peak of dodecane, since the solvent represents a high proportion of the product. In comparison to dodecane, the spectra differs in two weak bands around 3700 cm^{-1} and 1070 cm^{-1} which are related to O—H stretching vibration in primary alcohols.

The FTIR results from fresh microalgae on Fig. 8b displayed intense bands in the range of 3700–3050, 3050–2080, characteristic for lipids, 1457–1766 cm^{-1} characteristic for protein, and 1181–801 cm^{-1} characteristic for polysaccharides. Spectra is characterized by a strong peak at 1020 cm^{-1}, which is related to C–O–C vibrations in polysaccharides. Adsorption peaks at 1650 cm^{-1} and 1538 cm^{-1} can confirm the presence of proteins. The first band is related to C=O stretching vibrations in amide I, while the second is related to a combination of N–H bending and C–H stretching in amide II. C=O group in esters is seen at 1745 cm^{-1}. The adsorption band at 2925 cm^{-1} is characteristic for CH_2 vibration in lipids. Wide band with the peak at 3296 cm^{-1} corresponds to O–H stretching vibrations in water or N–H stretching vibrations in protein [10,42]. Liquefaction is evidenced in the spectra of solid residue (Fig. 8b) by the diminishing areas of all the peaks.

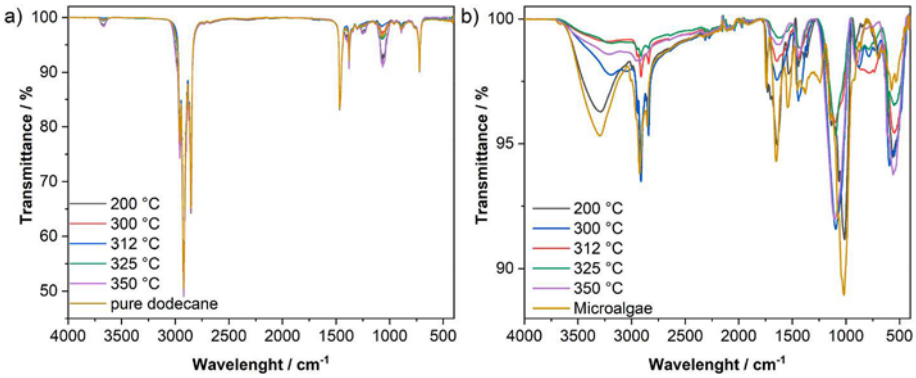

Fig. 8. FTIR spectra of a) produced oils at different temperatures and 50 bar compared to pure dodecane and b) solid residue produced at different temperatures and 50 bar compared to fresh feedstock.

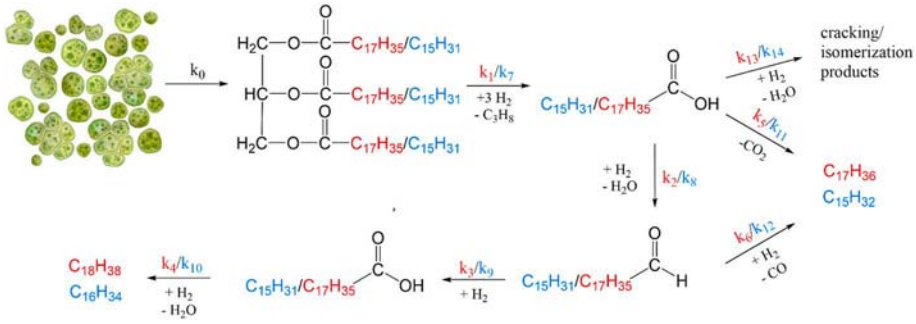

Fig. 9. Proposed reaction scheme for liquefaction and hydrotreatment of microalgae over NiMo/Al_2O_3 catalyst.

3.10. Reaction mechanism and model development

Detected intermediates produced by hydrodeoxygenation gave a detailed insight into the investigated reaction pathway, allowing us to develop a reaction scheme in accordance with the literature [17,22] (Fig. 9). The conversion of biomass to biofuels is a set of several different heterogeneous reactions.

Liquefaction and hydrotreatment were studied experimentally and modeled numerically. Experimental component concentrations were calculated using gas chromatography according to the calibration curves, while the modeled concentrations were determined through a series of differential equations in Matlab R2021a with ODE 23tb solver based on the implicit Runge-Kutta formula. The conversion of microalgae over solid catalyst with hydrogen was performed in a three-phase reactor. The model predicted that 1000 rpm would be a sufficient stirring speed in order to suppress external mass transfer limitations and the small catalyst particle size of 40–100 μm would overcome internal mass transfer limit. As the microalgae are natural biomass with countless components, the model is simplified and it considers only the main fatty acids present in the initial biomass, the main intermediates and products formed.

The reaction rate constant is determined by the transport phenomena involved in liquefaction process, mass transfer flux of hydrogen from gaseous to the liquid phase, adsorption and desorption of all components on/from the catalyst surface and their conversion on the catalyst surface. The mass balance for unliquefied and liquefied microalgae biomass can be described with the following differential equations:

$$\frac{dc_s}{dt} = -k_o \cdot c_s \cdot (c^* - c_d) \tag{7}$$

$$\frac{dc_d}{dt} = k_o \cdot c_s \cdot (c^* - c_d) - \sum_i^I \left(\pm r_i^{cat}\right) \tag{8}$$

In Eq. (7) and Eq. (8), c_s represents the mass concentration of unliquefied biomass, c^* equilibrium substrate concentration, c_d the mass concentration of liquefied biomass, k_o represents the kinetic constant of liquefaction and rate expressions (r_i^{cat}) for all the reactions i (I is the number of reaction) are defined in Eqs. (14) and (15).

Hydrogen is transferred from gas to liquid phase through dispersed bubbles. Its intrinsic concentration (c_{H2}^i) was determined by the temperature-dependent Henry's constant (He = $459.64^{(-0.004258\ T)}$ [MPa]) and evaluated by the following equation,

$$c_{H2}^i = \frac{p_{H_2}^g}{\frac{He \cdot M_{dodecane}}{\delta_{dodecane}}} \tag{9}$$

where $p_{H_2}^g$ stands for partial hydrogen pressure, $M_{dodecane}$ stands for molar mass of dodecane, and $\delta_{dodecane}$ stands for density of dodecane.

The mass transfer rates of hydrogen ($r_{H_2}^{GL}$) from gas (V_g) to liquid phase (V_l), where the interface area (a_g) for hydrogen was already determined in our previous article [43], is defined as follows:

$$r_{H_2}^{GL} = k_{H_2}^g \cdot a_g \cdot \left(c_{H2i}^i - c_{H_2^l}^l\right) \cdot \frac{V_l}{V_g} \tag{10}$$

We assumed that the adsorption rates (r_n^{ads}) of each compound n were much faster than the desorption rates (r_n^{des} and were calculated as:

$$r_n^{ads} = k_n^{ads} \cdot c_n^l \cdot c_{as} \tag{12}$$

$$r_n^{des} = k_n^{des} \cdot c_n^{ads} \cdot n_{TS} \tag{13}$$

In Eq. (12), k_n^{ads} represents adsorption rate constant, c_n^l concentration of the reactant in the liquid phase, c_{as} represent the concentration of active vacant sites. In Eq. (13), k_n^{des} represents kinetic constant for desorption and c_n^{ads} concentration of adsorbed reactant on the catalyst surface. The total concentration of active sites on the catalyst surface (n_{TS}) was

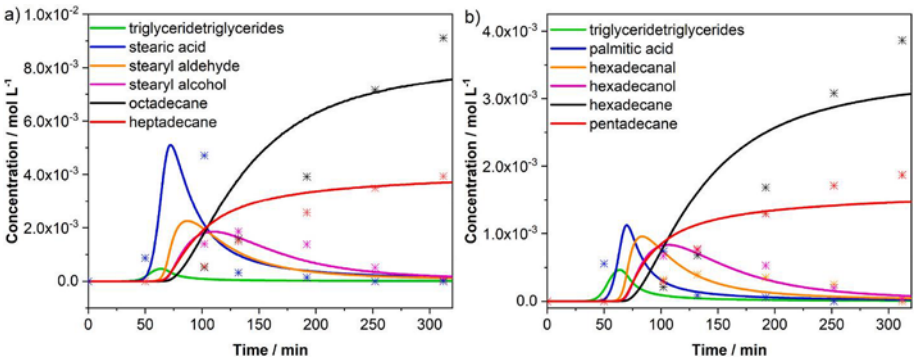

Fig. 10. Experimental data (*) and modeling results (lines) for hydrotreatment of microalgae at 350 °C and 50 bar of hydrogen for a) *triglycerides, *stearic acid, *stearyl aldehyde, *stearyl alcohol, *C18, *C17 and b) *triglycerides, *palmitic acid, *hexadecanal, *hexadecanol, *C16, *C15.

determined by the active sites, BET surface area and the catalyst mass.

The chemical transformations that took place on the catalyst surface and its kinetic rates (r_i^{cat}) for each compound i depend on kinetic rate constant (k_i^{cat}) besides its concentration in liquid phase (c_n^{ads}), and were defined as follows:

$$r_i^{cat} = k_i^{cat} \cdot c_n^{ads} \cdot n_{TS} \tag{14}$$

In the case of HDO and DCX, surface reaction rate also depends on the hydrogen adsorbed on the active sites (c_{H2}^{ads}).

$$r_i^{cat} = k_i^{cat} \cdot c_n^{ads} \cdot c_{H2}^{ads} \cdot n_{TS} \tag{15}$$

While both adsorption and desorption were considered temperature independent, kinetic rate constant (k_i^{cat}) was calculated in accordance with the Arrhenius law in Eq. (16),

$$k_i^{cat}(T_2) = k_i^{cat}(T_1) \bullet \exp\left(\frac{Ea_i}{R}\left(\frac{1}{T_1} - \frac{1}{T_2}\right)\right) \tag{16}$$

Pre-exponential factors (k_i^{cat}) and activation energies of reactions (Ea_i) were calculated with fitting the mathematical model to experimental data with the least square approximation method based on the Nelder-Mead simplex algorithm (Eq. (17)).

$$f(k_{i-n}, Ea_{i-n}) = \sum \left(c_{exp} - c_{mod(k_{i-n}, Ea_{i-n})}\right)^2 \tag{17}$$

Molar balances for hydrogen in gaseous phase ($n_{H_2}^g$), hydrogen in liquid phase ($c_{H_2}^l$), together with reactants, intermediates and products in liquid phase (c_n^l) are listed below.

$$\frac{dn_{H_2}^g}{dt} = -r_{H_2}^{GL} \tag{18}$$

$$\frac{dc_{H_2}^l}{dt} = r_{H_2}^{GL} - r_{H_2}^{ads} + \frac{r_{H_2}^{des}}{V_l} \tag{19}$$

$$\frac{dc_n^l}{dt} = -r_n^{ads} + \frac{r_n^{des}}{V_l} \tag{20}$$

The coverage of active sites for all the reactions i (I is the number of reaction) was balanced as follows:

$$\frac{dc_n^{ads}}{dt} = \left(r_n^{ads} \cdot V_l - r_n^{des} - \sum_i^I \left(\pm r_i^{cat}\right)\right) \Big/ nTS \tag{21}$$

General balance for concentration of vacant sites for all the compounds n (N is the number of compounds) that adsorb and desorb on/from the catalyst surface that have unstoichiometric balance of sites:

$$\frac{dc_{as}}{dt} = \left(\sum_n^N r_n^{des} - \sum_n^N r_n^{ads} \cdot V_l + \sum_i^I \left(\pm r_i^{cat}\right)\right) \Big/ nTS \tag{22}$$

Figs. 10 and 11 show the experimental (symbols) and modeled (lines) concentration profiles of the reactants, intermediates and products in the liquid phase against reaction time, for the reaction temperature of 350 °C. Kinetic parameters are presented in Table 5. The adequate agreement between model predictions and experimental results confirms the assumed reaction mechanism. However, the error was predictable. Only the main FAs in the feedstock, principal intermediates and products detected by GC were considered. Several liquid products

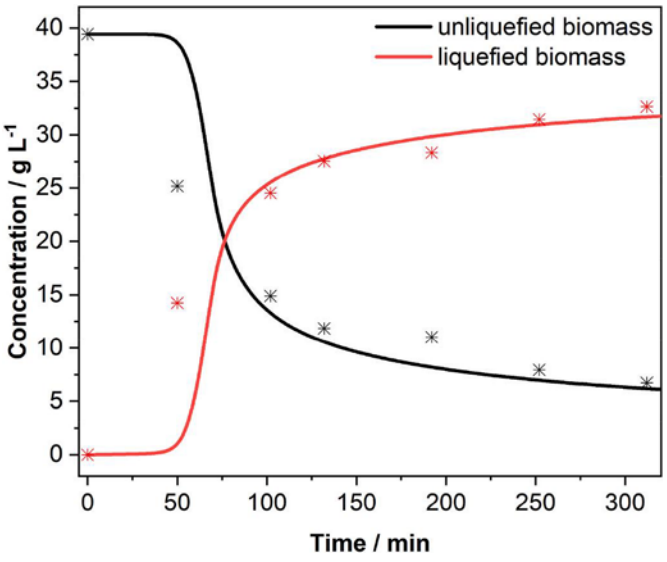

Fig. 11. Experimental data (*) and modeling results (lines) for liquefaction of microalgae at 350 °C and 50 bar of hydrogen.

Table 5
Kinetic constants and activation energies for surface reactions and liquefaction.

i	k_i^{cat} (T = 325 °C) [min^{-1}]	Ea_i [kJ•mol^{-1}]
0	1.93×10^{-6}	95
1	2.00×10^{2}	78
2	7.21×10^{0}	161
3	1.55×10^{1}	86
4	1.61×10^{1}	128
5	7.45×10^{-1}	164
6	2.72×10^{0}	154
7	4.99×10^{1}	93
8	1.50×10^{1}	171
9	1.69×10^{1}	78
10	8.45×10^{0}	113
11	1.68×10^{0}	168
12	2.97×10^{0}	111
13	2.67×10^{1}	65
14	2.02×10^{1}	72

were probably undetectable by GC due to high boiling point. Typical bio-oil compounds can also be formed from carbohydrates and proteins through hydrolysis and repolymerization, which the model has not considered.

Liquefaction is enhanced by the small size of microalgae, which has a highly beneficial impact on thermal transfer. However, the lowest rate constant exhibits the liquefaction of the microalgae to TG ($k_0 = 1.93 \times 10^{-6}$ min^{-1}), indicating the first reaction occurs relatively slow. Rapid hydrogenation of unsaturated FA units in the initial TG feedstock, mostly linoleic, linoelaidic and vaccenic acid, was followed by hydrogenolysis to three fatty acids, mostly stearic and palmitic acid. The fast hydrogenolysis of TG to FA is again confirmed by high kinetic constants (k_1 of 200.2 min^{-1} and k_7 of 49.9 min^{-1}). FA were converted from respective TG through diglycerides and monoglicerydes intedmediates, which were not seen. This is probably because of their high boiling point, hence they cannot be detected by GC and due to unfrequent sampling in the early stages of reaction, which was disabled due to potential clogging of the sampling line. Furthermore, Yenumala et al. [17] as well as Hachemi and Murzin [21] concluded, that TG promptly convert to respective FA. The kinetic constants of TG conversion into diglyceride, monoglyceride and acid reported by Hachemi and Murzin [21] (5.12×10^{-1}, 7.41×10^{-1} and 1.09×10^{-1} min^{-1}, respectively) were of one order higher than for conversion of acid into aldehyde (7.50×10^{-2} min^{-1}). Their another conclusion was, that the reaction rates are much dependent on the carbon chain length. The reactions were carried out only at 300 °C, therefore the calculation of activation energy was not possible.

FAs were then subjected to three possible reaction pathways, HDO, DCN and DCX. FA with similar carbon number show similar behavior [21]. Yenumala et *al.* [17] reported similar rate constants for stearic and palmitic acid, indicating HDO independence on the fatty acid chain length.

HDO includes the reduction of carboxyl group in the fatty acids to aldehyde group and formation of water molecule as a side product. Rapid hydrodeoxygenation of hexadecanal (k_9, Ea_9) and stearyl aldehyde (k_3, Ea_3) led to formation of cetyl alcohol and stearyl alcohol, respectively. Aldehydes were observed in trace concentrations. High reactivity and instantaneous conversion to alcohols or alkanes does not allow possible desorption off of the catalyst surface [1]. The same conclusions were made by several different authors, who investigated the HDO of steric acid [1,19] and TG [17]. Cetyl alcohol and stearyl alcohol were subsequently dehydrated to alkenes and hydrogenated to alkanes, C16 and C18.

Alkanes are formed via another two possible reaction pathways, namely DCN and DCX. The first route removes oxygen atom from palmitic and stearic acid as CO_2 and generates aliphatic hydrocarbon with one less carbon number as the corresponding FA, C15 and C17. DCX needs hydrogen for the release of one mol of CO, which converts hexadecanal and stearyl aldehyde to C15 and C17. The dominant deoxygenation pathway cannot be determined only by the carbon number distribution of the targeted fraction but also by the gas analysis. H_2O, CO and CO_2 formation in the gaseous phase was confirmed and detected by micro-GC analysis. The gas composition is difficult to explain, because beside the main reactions other (such as methanation and water gas shift reaction) also take place and their ratio cannot be determined [22]. Taking into account the aforementioned aspects (carbon number distribution, gas composition and catalyst used), the formation of hydrocarbons followed HDO pathway predominately. HDO kinetic constants (k_2–k_4 and k_8–k_{10}) were higher than those for DCN (k_6 and k_{12}) and DCX (k_5 and k_{11}). The same trend was reported by Hachemi and Murzin [21], where the lowest rate constants were calculated for the DCX (in the range of 10^{-2} and 10^{-3} for C18 and C16, respectively, compared to ours in the range of 10^{-1} and 10^{0} for C18 and C16, respectively). Moreover, the activation energies for DCN (Ea_6 and Ea_{12} being 154 kJ mol^{-1} and 111 kJ mol^{-1}, respectively) and DCX (Ea_5 and Ea_{11} being 164 kJ mol^{-1} and 168 kJ mol^{-1}, respectively) are high.

Hydrocracking, cyclization and isomerization were also present in the reaction pathway, evidenced by light hydrocarbons present in the product. According to the experimental results, most of C3–C6 isomers are formed from FA. Solvent degradation and isomerization to n-hexane, butane, pentane, 3-methyl pentane, methyl cyclopentane, cyclonhexane, heptane, octane, nonane and decane, were also observed and taken into account.

A similar model has been used in our previous article [26]. An extensive research of microkinetics of hexanoic acid and other model compounds hydrodeoxygenation over sulfided $NiMo/Al_2O_3$ has been carried out. In comparison to the present research, where the highest activation energies were determined for the conversion of acids into aldehydes (161 kJ mol^{-1} and 171 kJ mol^{-1} for C18 and C16, respectively), the highest activation barrier was set for the conversion of hexanol into hexane (150 kJ mol^{-1}). Furthermore, the activation barrier for DNC process for C18 and C16 was 164 kJ mol^{-1} and 168 kJ mol^{-1}, respectively, while the activation barrier of hexanal conversion into pentane in DCN process was 140 kJ mol^{-1}. The activation barrier of hexanoic acid conversion into pentane in DCX process was not determined.

Another extensive kinetic study of hydrodeoxygenation of stearic acid was done by Arora et al. [19]. The activation barrier for conversion of C18 FA into aldehyde, DCN and DCX were much lower (22.3 ± 17.3 kJ mol^{-1}, 119 ± 30.2 kJ mol^{-1} and 90.7 ± 80.4 kJ mol^{-1}, respectively), while for aldehyde into alcohol was much higher (159 ± 31.8 kJ mol^{-1}).

4. Conclusion

To meet the anticipated higher demand for fuel and to diminish the impact of fossil fuels on the environment, extensive efforts have to be made to improve biofuel production technology. In the current study, *Chlorella sorokiniana* was directly processed into diesel range hydrocarbons (C15–C18) via hydroprocessing using commercial $NiMo/\gamma\text{-}Al_2O_3$ catalyst in batch reactor. This research strongly concludes that the conversion of microalgae biomass to diesel-like hydrocarbons can be directly achieved by simultaneous liquefaction, hydrogenolysis and reduction of oxygen functional groups. One step process eliminates additional need for biocrude upgrading and extra processing cost.

The present work contains a comprehensive investigation of the reaction temperature, pressure, time and catalyst form. It can be concluded that the variation of mentioned parameters had a noticeable influence on the reaction yield. In agreement with the Arrhenius law, the rate of conversion of reactants considerably increased with the increase in temperature. By elevating the reaction temperature from 300 to 350 °C, the yield of C18 increased from 4.7% to 26.1%, while at 200 °C the product appeared in only trace concentrations. The saturation at lower pressures cannot be fully reached, hence, the product mixtures contained alkene intermediates. The most favorable results were obtained at the reaction temperature of 350 °C and 50 bar of initial hydrogen pressure over sulfided catalyst.

Based on the experimental results, simplified reaction scheme was proposed. The formation of C18 and C16 alkanes suggested the removal of oxygen via hydrodeoxygenation, while C17 and C15 formation suggested the elimination of oxygen via decarboxylation and decarbonylation. The production of hydrocarbons from fatty acids followed hydrodeoxygenation pathway predominately. A kinetic model that considers also the first step in the process, microalgae liquefaction, was developed for the first time. Relevant kinetic parameters obtained by the regression analysis allowed the prediction of the optimal process conditions for yielding n-parrafins and can be used for process optimization. The highest activation energies were determined for the conversion of acids into aldehydes (161 kJ mol^{-1} and 171 kJ mol^{-1} for C18 and C16, respectively).

CRediT authorship contribution statement

Dana Marinič: Methodology, Software, Validation, Formal analysis, Investigation, Data curation, Writing – original draft, Visualization. **Miha Grilc:** Software, Writing – review & editing. **Brigita Hočevar:** Conceptualization, Validation, Investigation. **Florian Delrue:** Resources, Writing – review & editing. **Blaž Likozar:** Resources, Supervision, Funding acquisition.

Declaration of competing interest

The authors declare that they have no known competing financial interests or personal relationships that could have appeared to influence the work reported in this paper.

Data availability

Data will be made available on request.

Acknowledgements

This research was funded by the Slovenian Research Agency (ARRS) through Programme P2–0152 and the research projects J2-2492 and NC-0013. The authors also acknowledge Ms. Urška Kavčič and Ms. Lara Planinc for their excellent laboratory work. The authors are grateful to Mr. Žan Lavrič for any help regarding modelling. The authors of this study are also grateful to Sašo Gyergyek for TEM analysis, the Centre of Excellence in Nanoscience and Nanotechnology – Nanocenter for the use of Transmission Electron Microscope Jeol JEM-2100 and to Janvit Teržan for SEM analysis.

Appendix A. Supplementary data

Supplementary data to this article can be found online at https://doi.org/10.1016/j.renene.2022.12.055.

References

[1] I. Hachemi, N. Kumar, P. Maki-Arvela, J. Roine, M. Peurla, J. Hemming, J. Salonen, D.Y. Murzin, Sulfur-free Ni catalyst for production of green diesel by hydrodeoxygenation, J. Catal. 347 (2017) 205–221, https://doi.org/10.1016/j.jcat.2016.12.009.

[2] How competitive is biofuel production in Brazil and the United States?. www.iea.org/articles/how-competitive-is-biofuel-production-in-brazil-and-the-united-states, 2019 (accessed November 20, 2021).

[3] H. Vieira de Mendonça, P. Assemany, M. Abreu, E. Couto, A.M. Maciel, R.L. Duarte, M.G. Barbosa dos Santos, A. Reis, Microalgae in a global world: new solutions for old problems? Renew. Energy 165 (2021) 842–862, https://doi.org/10.1016/j.renene.2020.11.014.

[4] P.A. Setier Delrue, C. Sahut, L. Cournac, A. Roubaud, G. Peltier, A.K. Froment, An economic, sustainability, and energetic model of biodiesel production from microalgae, Bioresour. Technol. 111 (2012) 191–200, https://doi.org/10.1016/j.biortech.2012.02.020.

[5] J.K. Bwapwa, A. Anandraj, C. Trois, Possibilities for conversion of microalgae oil into aviation fuel: a review, Renew. Sustain. Energy Rev. 80 (2017) 1345–1354, https://doi.org/10.1016/j.rser.2017.05.224.

[6] D. Moreira, J.C.M. Pires, Atmospheric CO2 capture by algae: negative carbon dioxideemission path, Bioresour. Technol. 215 (2016) 371–379, https://doi.org/10.1016/j.biortech.2016.03.060.

[7] C. Yang, B. Zhang, R. Li, Q. Qiu, Hydroprocessing catalysts for algal biofuels, in: Hydroprocessing Catal. Process., World Scientific, London, 2018, pp. 129–173.

[8] C. Yang, R. Li, C. Cui, S. Liu, Q. Qiu, Y. Ding, Y. Wu, B. Zhang, Catalytic hydroprocessing of microalgae-derived biofuels: a review, Green Chem. 18 (2016) 3684–3699, https://doi.org/10.1039/c6gc01239f.

[9] C. Hognon, F. Delrue, J. Texier, M. Grateau, S. Thiery, H. Miller, A. Roubaud, Comparison of pyrolysis and hydrothermal liquefaction of Chlamydomonas reinhardtii. Growth studies on the recovered hydrothermal aqueous phase, Biomass Bioenergy 73 (2015) 23–31, https://doi.org/10.1016/j.biombioe.2014.11.025.

[10] C.V. Viegas, I. Hachemi, S.P. Freitas, P. Maki-Arvela, A. Aho, J. Hemming, A. Smeds, I. Heinmaa, F.B. Fontes, D.C. da S. Pereira, N. Kumar, D.A.G. Aranda, D. Y. Murzin, A route to produce renewable diesel from algae: synthesis and characterization of biodiesel via in situ transesterification of Chlorella alga and its catalytic deoxygenation to renewable diesel, Fuel 155 (2015) 144–154, https://doi.org/10.1016/j.fuel.2015.03.064.

[11] G. Muhammad, A.D.P. Ngatcha, Y. Lv, W. Xiong, Y.A. El-Badry, E. Asmatulu, J. Xu, M.A. Alam, Enhanced biodiesel production from wet microalgae biomass optimized via response surface methodology and artificial neural network, Renew. Energy 184 (2022) 753–764, https://doi.org/10.1016/j.renene.2021.11.091.

[12] T.-H. Kim, K. Lee, M.Y. Kim, Y.K. Chang, M. Choi, Effects of fatty acid compositions on heavy oligomer formation and catalyst deactivation during deoxygenation of triglycerides, ACS Sustain. Chem. Eng. 6 (2018) 17168–17177, https://doi.org/10.1021/acssuschemeng.8b04552.

[13] A.B. Patrick Biller, Brajendra K. Sharma, Bidhya Kunwar, Hydroprocessing of bio-crude from continuous hydrothermal liquefaction of microalgae, Fuel 159 (2015) 197–205, https://doi.org/10.1016/j.fuel.2015.06.077.

[14] A. Ali, C. Zhao, Ru nanoparticles supported on hydrophilic mesoporous carbon catalyzed low-temperature hydrodeoxygenation of microalgae oil to alkanes at aqueous-phase, Chin. J. Catal. 41 (2020) 1174–1185, https://doi.org/10.1016/S1872-2067(20)63539-2.

[15] D. Valencia, I. Garcia-Cruz, V.H. Uc, L.F. Ramirez-Verduzco, M.A. Amezcua-Allieri, J. Aburto, Unravelling the chemical reactions of fatty acids and triacylglycerides under hydrodeoxygenation conditions based on a comprehensive thermodynamic analysis, Biomass Bioenergy 112 (2018) 37–44, https://doi.org/10.1016/j.biombioe.2018.02.014.

[16] P. Arora, H. Abdolahi, Y.W. Cheah, M.A. Salam, E.L. Grennfelt, H. Radberg, D. Creaser, L. Olsson, The role of catalyst poisons during hydrodeoxygenation of renewable oils, Catal. Today 367 (2021) 28–42, https://doi.org/10.1016/j.cattod.2020.10.026.

[17] S.R. Yenumala, S.K. Maity, S. Debaprasad, Reaction mechanism and kinetic modeling for the hydrodeoxygenation of triglycerides over alumina supported nickel catalyst, React. Kinet. Mech. Catal. 120 (2017) 109–128, https://doi.org/10.1007/s11144-016-1098-2.

[18] V.K. Soni, P.R. Sharma, G. Choudhary, S. Pandey, R.K. Sharma, Ni/Co-Natural clay as green catalysts for microalgae oil to diesel-grade hydrocarbons conversion, ACS Sustain. Chem. Eng. 5 (2017) 5351–5359, https://doi.org/10.1021/acssuschemeng.7b00659.

[19] P. Arora, E.L. Grennfelt, L. Olsson, D. Creaser, Kinetic study of hydrodeoxygenation of stearic acid as model compound for renewable oils, Chem. Eng. J. 364 (2019) 376–389, https://doi.org/10.1016/j.cej.2019.01.134.

[20] B. Yoosuk, P. Sanggam, S. Wiengket, P. Prasassarakich, Hydrodeoxygenation of oleic acid and palmitic acid to hydrocarbon-like biofuel over unsupported Ni-Mo and Co-Mo sulfide catalysts, Renew. Energy 139 (2019) 1391–1399, https://doi.org/10.1016/j.renene.2019.03.030.

[21] I. Hachemi, D.Y. Murzin, Kinetic modeling of fatty acid methyl esters and triglycerides hydrodeoxygenation over nickel and palladium catalysts, Chem. Eng. J. 334 (2018) 2201–2207, https://doi.org/10.1016/j.cej.2017.11.153.

[22] S. Kovacs, T. Kasza, A. Thernesz, I.W. Horvath, J. Hancsok, Fuel production by hydrotreating of triglycerides on NiMo/Al2O3/F catalyst, Chem. Eng. J. 176–177 (2011) 237–243, https://doi.org/10.1016/j.cej.2011.05.110.

[23] P. Agarwal, S.S. Al-Khattaf, M.T. Klein, Molecular-level kinetic modeling of triglyceride hydroprocessing, Energy Fuel. 33 (2019) 7377–7384, https://doi.org/10.1021/acs.energyfuels.9b01309.

[24] M. Grilc, B. Likozar, J. Levec, Hydrodeoxygenation and hydrocracking of solvolysed lignocellulosic biomass by oxide, reduced and sulphide form of NiMo, Ni, Mo and Pd catalysts, Appl. Catal., B 150–151 (2014) 275–287, https://doi.org/10.1016/j.apcatb.2013.12.030.

[25] M. Grilc, B. Likozar, J. Levec, Simultaneous liquefaction and hydrodeoxygenationof lignocellulosic biomass over NiMo/Al2O3, Pd/Al2O3, and zeolite YCatalysts in hydrogen donor solvents, ChemCatChem 8 (2016) 180–191, https://doi.org/10.1002/cctc.201500840.

[26] B. Hocevar, M. Grilc, M. Huš, B. Likozar, Mechanism, ab initio calculations and microkinetics of straight-chain alcohol, ether, ester, aldehyde and carboxylic acid hydrodeoxygenation over Ni-Mo catalyst, Chem. Eng. J. 359 (2019) 1339–1351, https://doi.org/10.1016/j.cej.2018.11.045.

[27] M. Grilc, B. Likozar, Levulinic acid hydrodeoxygenation, decarboxylation and oligmerization over NiMo/Al2O3 catalyst to bio-based value-added chemicals: modelling of mass transfer, thermodynamics and micro-kinetics, Chem. Eng. J. 330 (2017) 383–397, https://doi.org/10.1016/j.cej.2017.07.145.

[28] J. Liu, C. Liu, G. Zhou, S. Shen, L. Rong, Hydrotreatment of Jatropha oil over NiMoLa/Al2O3 catalyst, Green Chem. 14 (2012) 2499–2505, https://doi.org/10.1039/c2gc35450k.

[29] A.M. Lizzul, A. Lekuona-Amundarain, S. Purton, L.C. Campos, Characterization of chlorella sorokiniana, UTEX 1230, Biology 7 (2018) 1–12, https://doi.org/10.3390/biology7020025.

[30] H.-S. Yun, Y.-S. Kim, H.-S. Yoon, Characterization of Chlorella sorokiniana and Chlorella vulgaris fatty acid components under a wide range of light intensity and growth temperature for their use as biological resources, Heliyon 6 (2020), e04447, https://doi.org/10.1016/j.heliyon.2020.e04447.

[31] M. Axelsson, F. Gentili, A single-step method for rapid extraction of total lipids from green microalgae, PLoS One 9 (2014), https://doi.org/10.1371/journal.pone.0089643.

[32] M. Dubois, K.A. Gilles, J.K. Hamilton, P.A. Rebers, F. Smith, Colorimetric method for determination of sugars and related substances, Anal. Chem. 28 (1956) 350–356.

[33] D.W. Templeton, L.M.L. Laurens, Nitrogen-to-protein conversion factors revisited for applications of microalgal biomass conversion to food, feed and fuel, Algal Res. 11 (2015) 359–367, https://doi.org/10.1016/j.algal.2015.07.013.

[34] Y.K.C. Tae-Hyoung Kim, Kyungho Lee, Baek-Rock Oh, Mi-Eun Lee, Minji Seo, Sheng Li, Jae-Kon Kim, Minkee Choi, A novel process for the coproduction of biojet fuel and high-value polyunsaturated fatty acid esters from heterotrophic

microalgae Schizochytrium sp. ABC101, Renew. Energy 165 (2021) 481–490, https://doi.org/10.1016/j.renene.2020.09.116.
[35] S. Taipale, U. Strandberg, E. Peltomaa, A.W.E. Galloway, A. Ojala, M.T. Brett, Fatty acid composition as biomarkers of freshwater microalgae: analysis of 37 strains of microalgae in 22 genera and in seven classes, Aquat. Microb. Ecol. 71 (2013) 165–178, https://doi.org/10.3354/ame01671.
[36] L. Boda, G. Onyestyak, H. Solt, F. Lonyi, J. Valyon, A. Thernesz, Catalytic hydroconversion of tricaprylin and caprylic acid as model reaction for biofuel production from triglycerides, Appl. Catal. Gen. 374 (2010) 158–169, https://doi.org/10.1016/j.apcata.2009.12.005.
[37] P. Kumar, S.R. Yenumala, S.K. Maity, D. Shee, Kinetics of hydrodeoxygenation of stearic acid using supported nickel catalysts: effects of supports, Appl. Catal. Gen. J. 471 (2014) 28–38, https://doi.org/10.1016/j.apcata.2013.11.021.
[38] M. Snare, I. Kubickova, P. Maki-Arvela, K. Eranen, D.Y. Murzin, Heterogeneous catalytic deoxygenation of stearic acid for production of biodiesel, Ind. Eng. Chem. Res. 45 (2006) 5708–5715, https://doi.org/10.1021/ie060334i.
[39] B. Peng, Y. Yao, C. Zhao, J.A. Lercher, Towards quantitative conversion of microalgae oil to diesel-range alkanes with bifunctional catalysts, Angew. Chem. 51 (2012) 2072–2075, https://doi.org/10.1002/anie.201106243.
[40] K. Sun, , A.W. R., S.T. Thompson, H.H. Lamb, Catalytic deoxygenation of octanoic acid over supported palladium: effects of particle size and alloying with gold, ACS Catal. 5 (2015) 1939–1948.
[41] E.W. Ping, R. Wallace, J. Pierson, T.F. Fuller, C.W. Jones, Highly dispersed palladium nanoparticles on ultra-porous silica mesocellular foam for the catalytic decarboxylation of stearic acid, Microporous Mesoporous Mater. 132 (2010) 174–180, https://doi.org/10.1016/j.micromeso.2010.02.017.
[42] I. Ponnuswamy, S. Madhavan, S. Shabudeen, Isolation and Characterization green microalgae for Carbon Sequestration Waste water treatment and bio-fuel production, Int. J. Bio-Sci. Bio-Technol. 5 (2013) 17–26.
[43] B. Hocevar, M. Grilc, M. Hus, B. Likozar, Mechanism, ab initio calculations and microkinetics of hydrogenation, hydrodeoxygenation, double bond migration and cis–trans isomerisation during hydrotreatment of C6 secondary alcohol species and, Appl. Catal., B 218 (2017) 147–162, https://doi.org/10.1016/j.apcatb.2017.06.046.